Protein Expression and Purification 71 (2010) 33–41

Contents lists available at ScienceDirect

Protein Expression and Purification

journal homepage: www.elsevier.com/locate/yprep

Bioinformatic mapping and production of recombinant N-terminal domains of human cardiac ryanodine receptor 2

Vladena Bauerová-Hlinková [a,d], Eva Hostinová [a], Juraj Gašperík [a], Konrad Beck [c], Ľubomír Borko [a], F. Anthony Lai [d], Alexandra Zahradníková [a,b], Jozef Ševčík [a,*]

[a] Department of Protein Structure and Function, Institute of Molecular Biology, Slovak Academy of Sciences, Dúbravská Cesta 21, 845 51 Bratislava, Slovakia
[b] Laboratory of Molecular Biophysics, Institute of Molecular Physiology and Genetics, Center of Excellence for Cardiovascular Research, Slovak Academy of Sciences, Vlárska 5, 833 34 Bratislava, Slovakia
[c] Cardiff University School of Dentistry, Cardiff CF14 4XY, UK
[d] Department of Cardiology, Wales Heart Research Institute, Cardiff University School of Medicine, Cardiff CF14 4XN, UK

ARTICLE INFO

Article history:
Received 24 September 2009
and in revised form 18 December 2009
Available online 4 January 2010

Keywords:
Human cardiac ryanodine receptor 2 (RyR2)
Calcium release channel
Recombinant expression
Bioinformatics prediction
Proteolytic digestion

ABSTRACT

We report the domain analysis of the N-terminal region (residues 1–759) of the human cardiac ryanodine receptor (RyR2) that encompasses one of the discrete RyR2 mutation clusters associated with catecholaminergic polymorphic ventricular tachycardia (CPVT1) and arrhythmogenic right ventricular dysplasia (ARVD2). Our strategy utilizes a bioinformatics approach complemented by protein expression, solubility analysis and limited proteolytic digestion. Based on the bioinformatics analysis, we designed a series of specific RyR2 N-terminal fragments for cloning and overexpression in *Escherichia coli*. High yields of soluble proteins were achieved for fragments RyR2$^{1-606}$·His$_6$, RyR2$^{391-606}$·His$_6$, RyR2$^{409-606}$·His$_6$, Trx·RyR2$^{384-606}$·His$_6$, Trx·RyR2$^{391-606}$·His$_6$ and Trx·RyR2$^{409-606}$·His$_6$. The folding of RyR2$^{1-606}$·His$_6$ was analyzed by circular dichroism spectroscopy resulting in α-helix and β-sheet content of ~23% and ~29%, respectively, at temperatures up to 35 °C, which is in agreement with sequence based secondary structure predictions. Tryptic digestion of the largest recombinant protein, RyR2$^{1-606}$·His$_6$, resulted in the appearance of two specific subfragments of ~40 and 25 kDa. The 25 kDa fragment exhibited greater stability. Hybridization with anti-His$_6$·Tag antibody indicated that RyR2$^{1-606}$·His$_6$ is cleaved from the N-terminus and amino acid sequencing of the proteolytic fragments revealed that digestion occurred after residues 259 and 384, respectively.

The ryanodine receptor (RyR) is the calcium release channel responsible for excitation–contraction coupling in mammalian muscle cells[1]. It is a huge homotetrameric protein with a molecular weight of 565 kDa per subunit [1]. Approximately 90% of the RyR polypeptide chain forms a bulky cytoplasmic domain that modulates Ca^{2+} channel function. The remaining 10% (C-terminal region) constitutes the transmembrane and the channel pore-forming regions [2]. The RyR2 isoform is predominant in cardiac muscle, where it plays a crucial role in providing the calcium for contraction by the process of calcium-induced calcium release [3]. The N-terminal and the central regions of the skeletal and cardiac ryanodine receptor isoforms (RyR1 and RyR2) contain specific amino acid residues, whose mutations cause malignant hyperthermia [4] and central core disease [5] in skeletal muscle, and catecholaminergic polymorphic ventricular tachycardia (CPVT1, [6]) or arrhythmogenic right ventricular dysplasia (ARVD2, [7]) in cardiac muscle. These diseases have a phenotypic signature suggesting a tendency to hyper-activation of RyRs under certain conditions [8]. The unique distribution of these mutation sites has led to the concept that interaction between domains of the N-terminal and central region within the RyR may play a key role in regulating channel opening [8,9]. Indeed, the addition of short synthetic peptides corresponding to the mutation-prone regions of RyR1 and RyR2 leads to increased activation of RyRs, suggesting that the interaction between these two domains is required for proper channel closure [9–11]. Consequently, defective interdomain interaction has been hypothesized to be involved also in the dysfunction of wild-type RyR2 channels in heart failure [12]. Recently, the tertiary structures of N-terminal domains of the rabbit and mouse RyR1 (aa residues 1–210 and 9–205) [13,14], and the

* Corresponding author. Fax: +4212 5930 7416.
E-mail address: jozef.sevcik@savba.sk (J. Ševčík).

[1] Abbreviations used: aa, amino acid; ARVD2, arrhythmogenic right ventricular dysplasia; CD, circular dichroism; CPVT 1, catecholaminergic polymorphic ventricular tachycardia; IMAC, immobilized metal affinity chromatography; Ins1_45_P3_Rec, inositol 1,4,5-trisphosphate/ryanodine receptor; IPTG, isopropyl β-D-1-thiogalactopyranoside; IP3R, inositol trisphosphate receptor; LIZ, leucine/isoleucine zipper region; MIR, a domain found in mannosyltransferase, IP3R and RyR, PP1, protein phosphatase; PAGE, polyacrylamide gel electrophoresis; RIH, a domain found in RyR and IP3R; RyR2, human cardiac ryanodine receptor; SDS, sodium dodecyl sulfate; SPI, spinophilin, Trx; thioredoxin; Tris, tris(hydroxymethyl)aminomethane.

1046-5928 © 2010 Elsevier Inc. Open access under CC BY-NC-ND license.
doi:10.1016/j.pep.2009.12.014

mouse RyR2 (aa residues 1–217) [14] were solved. The structures contain MIR domains and adopt a β-trefoil fold, similar to IP3R.

Human cardiac RyR2 cDNA has been available for more than 15 years [2]. Due to the complex structure of this channel protein; however, many functions of the discrete RyR2 domains, prepared by recombinant techniques, have not been analyzed yet. The recombinant proteins are often used to obtain sufficient amount of material for biological experiments. The many advantages of *Escherichia coli* have ensured that it remains the expression system of choice for high-level production of heterologous proteins [15]. In general, *E. coli* is the preferred host for recombinant protein production for structural studies [16,17]. *E. coli* is favored because it has well characterized, relatively simple genetics and a rapid growth rate [18]. However, a disadvantage of expressing foreign proteins in *E. coli* is that these are often produced as insoluble "inclusion bodies". One way to reduce protein aggregation is due to self-association of the nascent polypeptide chains is to reduce the rate of protein synthesis in *E. coli* by applying lower growth temperatures [19,20]. The induction of gene expression at sub-optimal growth temperatures helps to minimize inclusion body formation [21]. Other parameters that may influence protein solubility are culture medium, time of induction, aeration and *E. coli* strain. Another successful approach in expressing soluble recombinant proteins in *E. coli* is the use of gene fusions. From a variety of structures available as fusion motifs, the *E. coli* proteins thioredoxin (Trx) and NusA are frequently used. NusA was found by screening for proteins with the highest potential for solubility when overexpressed [22].

Structural studies of the cardiac ryanodine receptor RyR2 based on cryoelectron microscopy [23] showed that the protein consists of several domains. Supposing that the arrhythmogenic mutations in the N-terminal part of RyR2 destabilize the protein [12], our strategy is aimed to analyze folding as well as the properties and the structure of N-terminal domains of human wild-type RyR2 fragments followed by comparison with mutated forms. Although the structure of a short N-terminal fragment of the mouse RyR2 (1–217) was solved recently [14], any human RyR2 fragment structure, especially one containing the mutation-rich region (aa 400–450 [24]), is of immense importance due to its medical significance.

In the present study, we report the bioinformatics structural prediction and consequent production of various recombinant human RyR2 fragments comprising the discrete domains present in the N-terminal region in *E. coli*. These fragments were designed on the basis of bioinformatics analysis and prediction of the secondary structure elements of the whole RyR2 protein. The expression level of the N-terminal RyR2 fragments was tested at a range of temperatures and low-induction conditions to obtain soluble and properly folded products. The RyR2 fragments were synthesized either as authentic sequences fused at the C-terminus with an uncleavable His·Tag or as N-terminal fusions with NusA or Trx. The constructs that exhibited a detectable level of protein expression were analyzed for the presence of soluble recombinant products. Proteins obtained from IMAC chromatography were compared with those forming insoluble particles. The largest N-terminal fragment of RyR2 (aa 1–606) was analyzed by circular dichroism (CD) spectroscopy and by tryptic digestion that generated two discrete proteolytic products.

Materials and methods

Construction of expression vectors

Plasmid BT4 carrying the N-terminal cDNA sequence (aa 1–759) [25] of the human cardiac muscle ryanodine receptor RyR2 (EMBL accession no. X98330) served as a DNA template. Platinum Pfx DNA polymerase (Invitrogen, Carlsbad, CA) and Taq DNA polymerase (Promega, Madison, WI) were used for PCR amplification of various fragments of interest and for introduction of the appropriate restriction sites (Table 1). PCR products were purified using the QIAquick PCR Purification Kit (Qiagen, Hilden, Germany) and subcloned into pET28a, pET32a and pET50b vectors (Novagen – Merck Biosciences, Darmstadt, Germany). *E. coli* TG1 was used for cloning and vector amplification. To all RyR2 fragments cloned into pET28a and pET32a vectors, hexahistidine tags (His_6) were added at the C-terminus as an uncleavable fusion. Fragments cloned into pET50b, with N-terminal NusA protein fusion, had two His_6·Tags: one at the N-terminus, before the NusA protein, and a second one between NusA and the RyR2 fragment. The cloning strategy into pET28a and pET32a used NcoI and BamHI restriction sites upstream and downstream of the coding sequence, respectively. For cloning into pET50b, BamHI and SalI sites upstream and downstream of the coding sequence were used, respectively. All constructs were verified by DNA sequencing.

Protein expression screening

Medium-scale expressions of RyR2 fragments in *E. coli* BL21 (DE3) were performed in 100 ml Erlenmeyer flasks with 20 ml LB medium supplemented with the respective antibiotics (30 μg/ml of Kanamycin or 50 μg/ml Ampicillin) and inoculated to 1:100 dilution with over-night culture, grown at 30 °C. The cultivation started at 23 °C. When OD_{600} reached ~0.5–0.6, the temperature was reduced to 17 °C and protein expression was induced by 10 μM IPTG. A parallel cultivation without IPTG induction was performed as a negative control. After over-night cultivation, 1 ml of media was used for expression analysis on SDS–PAGE. The rest of

Table 1
Primer sequences used for cloning of RyR2 N-terminal fragments.

RyR2 fragment	DNA sequence
$RyR2^{1-606}$·His_6	F: 5′CC**CCATGG**CCGATGGGGGCGAGGGCGAA[*] R: 5′CC**GGATCC**TTAGTGATGATGATGATGATGTCTTCCATGTTTGTCTAAAAGTGAGATAATAG[**]
$RyR2^{1-223}$·His_6	R: 5′CC**GGATCC**TTAGTGATGATGATGATGTGCCT CACTTCCTGAGCTGATTGGGGCCAC
$RyR2^{1-247}$·His_6	R: 5′CC**GGATCC**TTAGTGATGATGATGATGGACAGT GAGACACTCGTCCATGTGTCCATGCAG
$RyR2^{1-382}$·His	R: 5′CC**GGATCC**TTAGTGATGATGATGATGCACGGA TTTCACGTCCACAGACTGGTAAGTAAG
$RyR2^{230-606}$·His_6	F: 5′ GG**CCATGG**GTGGTGATGTCCTCAGGTTGC
$RyR2^{384-606}$·His_6 Trx·$RyR2^{384-606}$·His_6	F: 5′GG**CCATGG**GATCTATACAACGTAAGGCTATTATG
$RyR2^{391-606}$·His_6 Trx·$RyR2^{391-606}$·His_6	F: 5′GG**CCATGG**CTCATGAAGGCCACATGGATGATGGC
$RyR2^{409-606}$·His_6 Trx·$RyR2^{409-606}$·His_6	F: 5′GG**CCATGG**CGCATGAAGAATCACGCACAGCCCG
Nus·$RyR2^{1-606}$	F: 5′GG**GGATCC**GGATGACGACGACAAGATGGCCGATG GGGGGCGAGGGCGAA R: 5′CC**GTCGAC**TTATCTTCCATGTTTGTCTAAAAGTGAG ATAATAGG
Nus·$RyR2^{230-606}$	F: 5′GG**GGATCC**GGATGACGACGACAAGGGTGGTGATGT CCTCAGGTTGCTG
Nus·$RyR2^{409-606}$	F: 5′GG**GGATCC**GGATGACGACGACAAGCAGCATGAA GAATCACGCACAGCCCG

F: forward; R: reverse; CCATGG, GGATCC and GTCGAC represent NcoI, BamHI and SalI restriction sites, respectively. If a forward primer is not indicated, ([*]) was used. If a reverse primer is not indicated, ([**]) was used.

the induced cells was pelleted by centrifugation (10,000*g* for 10 min at 4 °C), washed with 0.9% NaCl, frozen in liquid nitrogen and stored at −80 °C.

Cell lysis, protein extraction and purification

For obtaining the soluble recombinant protein, the following protocols were used:

(a) About 0.1 g of frozen cells (obtained from 20 ml of culture) was homogenized in 500 μl of BugBuster Master Mix (Novagen – Merck Biosciences, Darmstadt, Germany) Protease inhibitor Mix B (Serva, Nordmark, Germany) and incubated on ice for 30 min to obtain an optimal lysis of the cells.
(b) About 0.1 g of frozen cells homogenized in 500 μl of 50 mM Tris–HCl (pH 8.0), 300 mM NaCl, 10 mM imidazole, 7 mM β-mercaptoethanol containing protease inhibitor Mix B was sonicated for 15 s, then 60 μl of 10% Triton X-100 was added and stirred for 1 h at 4 °C. Insoluble cell debris (CD) was removed by centrifugation (16,000*g* for 30 min at 4 °C).

Supernatant containing the proteins from the periplasm and cytoplasm was applied to 100 μl of Ni-NTA His·Bind Resin (Novagen – Merck Biosciences, Darmstadt, Germany) equilibrated with 50 mM Tris–HCl (pH 8.0), 300 mM NaCl, 10 mM imidazole, 7 mM β-mercaptoethanol and mixed gently at 4 °C for 15 min. Then the resin was collected by centrifugation (100*g*, 30 s) and washed with 500 μl of the above buffer. The bound recombinant protein was eluted with 100 μl of elution buffer (50 mM Tris–HCl (pH 8.0), 400 mM imidazole, 7 mM β-mercaptoethanol) to obtain the soluble protein (SP). The purity of the RyR2 fragments was checked by SDS–PAGE. The presence of the monomeric form of RyR2 fragments was determined by gel filtration on calibrated Superdex 75, Superose 6 and 12, HR10/30 columns (FPLC system, Pharmacia, Sweden) equilibrated in 20 mM HEPES (pH 8.0), 0.1% Triton X-100, 7 mM β-mercaptoethanol.

Circular dichroism (CD) spectroscopy

CD spectra were recorded on an Aviv Model 215 spectropolarimeter (Aviv Biomedical Inc., Lakewood, NJ) equipped with a Peltier thermostatted cell holder. Far-UV spectra (260–178 nm) were collected in a 0.01-cm quartz cuvette at 4, 16, 20, 30, 35 and 40 °C at a protein concentration of ~20 μM with 4 s accumulation times per point at 0.2 nm intervals using a 1 nm bandwidth. Near-UV spectra (340–250 nm) were collected at 4 °C in a 0.1 cm cuvette ($c_{protein}$ ~80 μM) with 8 s per point/two scans at 0.2 nm intervals using a 0.5 nm bandwidth. Buffer baselines recorded in the same cell were subtracted, data were smoothed (Savitzky–Golay algorithm, ±2 points), and normalized to mean residue ellipticities $[\theta]_{MRW}$. The instrument was calibrated with camphorsulfonic acid [26].

To remove chloride ions, which strongly absorb at $\lambda < 195$ nm, the protein was dialyzed to 20 mM Tris·SO_4, pH 8.0, buffer containing 100 mM NaF, 0.1% Tween-20 at 4 °C. Samples were measured in the absence and presence of dithiothreitol (c_{final} = 0.5 mM) added 1 h before recording. Samples were kept on ice up to the transfer into the pre-cooled cuvette. To test for any effect on the secondary structure, far-UV spectra were recorded 30 min after the addition of ATP (Sigma Aldrich, Germany; 3 mM stock solution) to a 2.5 μM protein solution up to a 175 × molar excess of ATP. Protein concentration was determined from the absorption at 280 nm assuming an extinction coefficient of ε_{280} = 75,860 $M^{-1}cm^{-1}$ based on the amino acid composition [27]. CD spectra were deconvoluted for the secondary structure content using the CDsstr algorithm [28] as implemented in the Dichroweb server [29] with the SP175 reference data set [30].

Limited proteolysis by trypsin and chymotrypsin

For trypsin and chymotrypsin digestion, the soluble monomeric recombinant fragment $RyR2^{1-606}$·His_6 was used (1 mg/ml of protein dissolved in 50 mM Tris–HCl, (pH 7.5), 0.5% Triton X-100). Trypsin and chymotrypsin (Promega, Madison, WI) were dissolved in 50 mM Tris–HCl (pH 7.5) and used at a concentration of 0.01 mg/ml as recommended. The fragment $RyR2^{1-606}$·His_6 and added protease were mixed in a 2:1 ratio. Protease digestions at 25 °C lasting 5 and 10 min, respectively, for each enzyme was performed. After digestion the reaction was stopped by adding an equivalent amount of SDS sample buffer followed by boiling at 100 °C for 10 min. The products of proteolytic digestions were analyzed on 15% SDS–PAGE.

Immunodetection and N-terminal sequencing

For immunodetection of RyR2 fragments obtained after trypsin and chymotrypsin digestion, 3–7 μg of the digested protein were run on 15% SDS–PAGE and transferred to a 0.45 μm immobilon-P transfer membrane (Millipore, Billerica, MA) in the transfer buffer (10 mM $NaHCO_3$, 3 mM Na_2CO_3, 20% methanol, pH 9.9) at 350 mA (Mini Trans-Blot®, BioRad, Hercules, CA) for 55 min. The membrane was immunoblotted with His·Tag Monoclonal Antibody (1:1000; Novagen – Merck Biosciences, Darmstadt, Germany), followed by Anti-mouse IgG peroxidase conjugate antibody (1:5000; Sigma, Germany). The signals were detected on X-ray film (Kodak, USA) using ECL™ (Enhanced Chemoluminiscence Western Blotting System, Amersham Biosciences – GE Healthcare, Piscataway, NJ) according to the manufacturer's instructions.

The N-terminal amino acid sequences of the proteolytic digests obtained by trypsin were determined by Edman degradation using the Procise® Protein Sequencing System (PE Applied Biosystems, 491 Protein Sequencer).

Results and discussion

Bioinformatics prediction of RyR2 domains in the N-terminal region

In this study we were interested in mapping the N-terminal region of RyR2, amino acids 1–759, which includes one of the three mutation clusters associated with the heart diseases, ARVD2 and CPVT1 [8], and in preparing efficient expression systems for the production of soluble N-terminal RyR2 fragments. We combined bioinformatics analysis with protein expression, solubility analysis, CD spectroscopy, limited proteolysis and N-terminal amino acid sequencing.

To find the putative individual structural entities in the N-terminal region, we analyzed the whole RyR2 amino acid sequence using the PFAM domain database [31]. The PFAM prediction indicated 14 domains in the RyR2 monomer. Three of them were localized in the N-terminal region (aa residues 1–759) and were identified as Ins145_P3_Rec, MIR, and RIH. At the C-terminal end of this region (aa residues 670–759), part of a SPRY domain was also present (Fig. 1A). The Ins145_P3_Rec domain was found in RyRs, where its function is unknown [32], and in the inositol 1,4,5-trisphosphate receptor (IP3R), in which it participates in forming the ligand binding suppressor region [33]. The RIH domain was found in RyRs and IP3Rs. Structurally it is composed of α-helical and β-strand segments. In the IP3R, this domain forms the binding site for inositol 1,4,5-trisphosphate [34]. In RyR2, the RIH domain was reported to contain a leucine–isoleucine zipper between amino acid residues

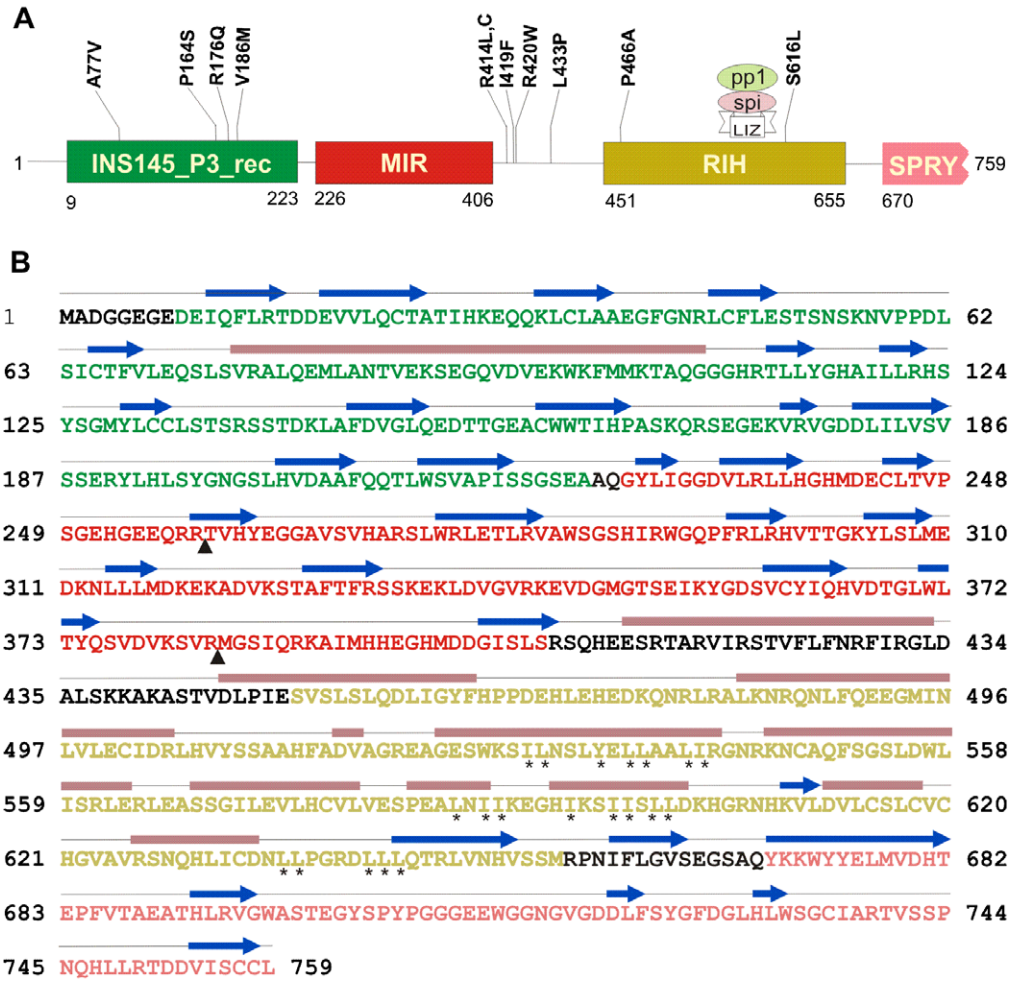

Fig. 1. **(A)** Domain prediction in the N-terminal fragment (amino acid residues 1-759) of the human cardiac RyR2 receptor by Pfam. Pfam analysis of this RyR2 N-terminal fragment indicates that it comprises an Ins145_P3_rec, MIR, RIH and part of a SPRY domain. Mutations of specific residues believed to be involved in ARVD2 and CPVT1 are shown. LIZ (amino acid residues 554-585) represents the leucine-isoleucine zipper area. SPI and PP1 represent spinophilin and protein phosphatase 1, respectively. Areas for LIZ, SPI and PP1 were adapted from Ref. [26]. **(B)** Secondary structure prediction of the N-terminal region (amino acid residues 1-759) of the human cardiac RyR2 receptor (program JPRED). Amino acids involved in Ins145_P3_Rec, MIR, RIH and SPRY domains according PFAM are in green, red, yellow and magenta colors, respectively. Interdomain regions are black. α-helices and β-strands are marked as purple bars and blue arrows, respectively. Areas rich in leucines and isoleucines are labeled with asterisks. The trypsin cleavage sites obtained by directed proteolysis are marked with black triangles.

554 and 585 that mediates binding of the phosphatase PP1 via the spinophilin targeting protein [35]. MIR domains, usually consisting of several MIR motifs, were found in several proteins: mannosyltransferase [36], IP3R [33,34], RyRs [32], eukaryotic stromal cell-derived factor 2 [37] and *Chlamydia trachomatis* protein CT153 [24]. In PMT1 mannosyltransferases, MIR motifs are located in the luminal loops of the enzyme and are essential for transferase activity [35]. The MIR motif consists of ~50 residues, and folds into the so-called β-trefoil fold [38], a closed beta-barrel structure with hairpin triplets and internal pseudo-threefold symmetry [33]. In the IP3R, the first two of the β-trefoil motifs were found to belong to the ligand binding suppressor region (INS145_P3_Rec, [34]), while the latter two (belonging to the MIR domain) formed a part of the ligand binding region [33]. Similar β-trefoil motifs were predicted to be present in the N-terminal region of the RyR1 isoform [34], and later found in the crystal structure of the RyR1 N-terminal domain [13], although the level of sequence similarity between IP3R and RyR is relatively low.

The above mentioned domains were further refined by prediction of secondary structure elements in JPRED [39], shown in Fig. 1B, and by amino acid sequence comparison with IP3R [33,34]. This prediction has clearly shown that there are two subregions, the first one containing mainly β-strands and involving domains Ins145_P3_rec and MIR, and the second one containing mainly α-helices and involving a large part of the RIH domain and the amino acids immediately preceding it.

Evaluation of expression of RyR2 fragments in E. coli

In spite of the clear PFAM prediction of RyR2 N-terminal domains, we decided to design several constructs covering the predicted domains with various alternatives at their N and C termini, considering the secondary structure elements and the known structure of the related IP3R domains (Table 2). All fragments were designed not to disrupt the predicted secondary structure elements. In six fragments, the methionines present in the RyR2 1–759 sequence were used as the starting residue.

The fragments $RyR2^{1-223}{\cdot}His_6$ and $RyR2^{1-247}{\cdot}His_6$ represent the Ins145_P3_Rec domain. The fragment $RyR2^{1-382}{\cdot}His_6$ contains the Ins145_P3_Rec and MIR domains. The fragment $RyR2^{230-606}{\cdot}His_6$ involves almost complete MIR and the core of RIH domains. The largest N-terminal RyR2 fragment $RyR2^{1-606}{\cdot}His_6$ involves all three putative N-terminal domains. The third domain, RIH, suggested by PFAM starts with Ser451. However, this residue is in the middle of a predicted α-helix, which is preceded by another α-helix and a loop (Fig. 1B). It appeared that a separate domain may start

Table 2
Constructs of N-terminal RyR2 fragments and their expression levels.

Construct	RyR2 fragments	Calculated M_W (kDa)	Vector	Cloning site	Protein expression
1	$RyR2^{1-223}$·His_6	25.4	pET 28a	NcoI, BamHI	–
2	$RyR2^{1-247}$·His_6	27.9	pET 28a	NcoI, BamHI	++
3	$RyR2^{1-382}$·His_6	43.3	pET 28a	NcoI, BamHI	–
4	$RyR2^{1-606}$·His_6	68.6	pET 28a	NcoI, BamHI	++
5	$RyR2^{230-606}$·His_6	43.5	pET 28a	NcoI, BamHI	–
6	$RyR2^{384-606}$·His_6	26.0	pET 28a	NcoI, BamHI	–
7	$RyR2^{391-606}$·His_6	25.2	pET 28a	NcoI, BamHI	++
8	$RyR2^{409-606}$·His_6	23.2	pET 28a	NcoI, BamHI	+++
9	Nus·$RyR2^{1-606}$	128.6	pET 50b	BamHI, SalI	++
10	Nus·$RyR2^{230-606}$	104	pET 50b	BamHI, SalI	++
11	Nus·$RyR2^{409-606}$	84.5	pET 50b	BamHI, SalI	–/++*
12	Trx·$RyR2^{384-606}$·His_6	43.3	pET 32a	NcoI, BamHI	+++
13	Trx·$RyR2^{391-606}$·His_6	42.5	pET 32a	NcoI, BamHI	+++
14	Trx·$RyR2^{409-606}$·His_6	40.5	pET 32a	NcoI, BamHI	+++

Quantification of expression: – undetectable expression level, ++ 1–5 mg/l g of expressed cells, +++ more than 5 mg/1 g of expressed cells. The amount of the protein was determined after IMAC purification.
* High expression of Nus·$RyR2^{409-606}$ was detected only with a high concentration of IPTG (0.5–1 mM) used for protein induction. With a low IPTG concentration (10–100 μM), no expression was detected.

before the β-strand. Based on this, we designed three fragments: $RyR2^{384-606}$·His_6, $RyR2^{391-606}$·His_6 and $RyR2^{409-606}$·His_6.

The constructs of the N-terminal RyR2 domains cloned and expressed in the pET28 vector produced products with an authentic N-terminus preceded with a methionine and terminated with His_6·Tag. We also expressed RyR2 fragments in N-terminal fusion with thioredoxin or NusA protein, which are known to significantly increase the solubility of the recombinant protein [40]. Expression of the recombinant RyR2 fragments was detected by SDS–PAGE from the cell lysate, as shown in Table 2.

Evaluation of the expressed products showed that nine out of 14 N-terminal RyR2 constructs (nos. 2, 4, 7, 8, 9, 10, 12, 13 and 14) gave proteins of the expected size (Fig. 2). The lack of expression in $RyR2^{230-606}$·His_6 and $RyR2^{341-606}$·His_6 (constructs 5 and 6, respectively) could have been caused by the presence of the rarely used *E. coli* codons at the very N-termini of the given fragments when expressed as authentic proteins. This problem was overcome by fusion with Nus or thioredoxin (constructs 10, 12).

Low cultivation temperature, below 20 °C, was found to be the critical condition for successful expression of soluble RyR2 fragments. Expression levels obtained at either 37 or 28 °C for the majority of the constructs were very low. We have also observed that in most cases a low concentration of IPTG (10 μM) and prolonged post-induction time (16 h) were important for good yields of soluble recombinant proteins. The best expression levels for the RyR2 fragments with authentic N-termini were obtained for the fragment $RyR2^{409-606}$·His_6 followed by the fragments $RyR2^{391-606}$·His_6 and $RyR2^{1-247}$·His_6. A lower expression level was found for the fragment $RyR2^{1-606}$·His_6 (Fig. 2A).

The fragments $RyR2^{1-606}$ and $RyR2^{230-606}$ fused with the NusA protein showed good expression levels as well, Fig. 2B. Interestingly, expression of NusA·$RyR2^{409-606}$ was detected only at the low temperature combined with a higher IPTG concentration (0.5–1 mM) for induction. Termination of all fragments at the residue Arg606 was important, as shortening of the C-terminus to Cys577 resulted in almost no expression.

High expression was obtained for the constructs prepared with thioredoxin fusions: Trx·$RyR2^{384-606}$·His_6, Trx·$RyR2^{391-606}$·His_6 and Trx·$RyR2^{409-606}$·His_6 Fig. 2C.

Evaluation of the solubility of RyR2 fragments

To address the question of whether the recombinant N-terminal RyR2 fragments can be prepared from *E. coli* in soluble, monomeric

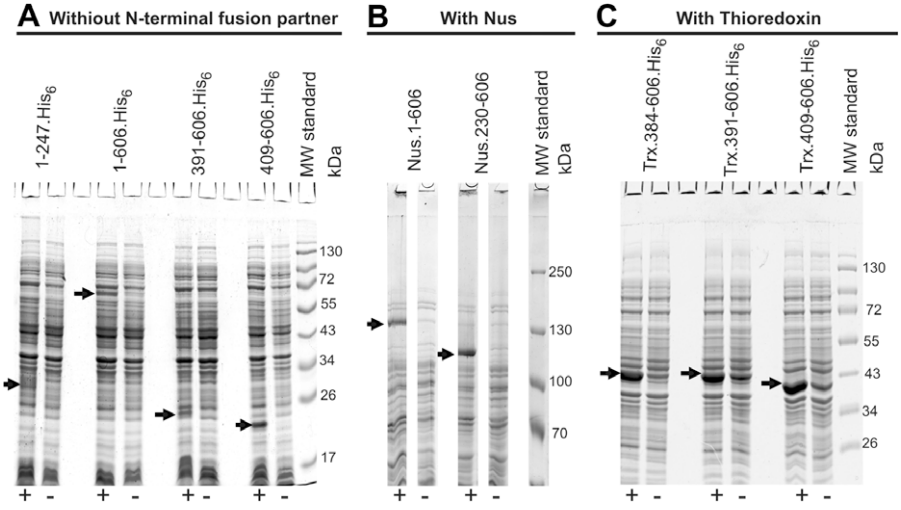

Fig. 2. Evaluation of expression of the N-terminal RyR2 fragments. Recombinant protein production (see Materials and methods and Table 2) was induced by 10 μM IPTG at 17 °C over-night. Proteins were resolved in 12% SDS–PAGE (A and C) or 7.5% SDS–PAGE (B), and compared with uninduced cells cultivated identically. Arrowheads indicate the positions of the expressed proteins. (+) and (–), induced and uninduced culture, respectively.

forms, the constructs nos. 2, 4, 7, 8, 9, 10, 12, 13 and 14 Table 2, were further analyzed. The IMAC technology based on affinity binding of the recombinant proteins carrying His·Tag from the soluble fraction of the lysed cells to Ni-NTA His·Bind Resin was used. The bound proteins, released from the resin with 400 mM imidazole (SP) were compared with those that remained in the insoluble cell debris (CD). In preliminary experiments using the constructs RyR2$^{1\text{-}247}$·His$_6$, RyR2$^{391\text{-}606}$·His$_6$, RyR2$^{409\text{-}606}$·His$_6$ and RyR2$^{1\text{-}606}$·His$_6$, two types of solubilization agents – BugBuster Protein Extraction Reagent (Novagen) and Triton X-100 were tested. As seen in Fig. 3A,B, BugBuster was an efficient solubilization agent; however, Triton X100 was more selective for the recombinant RyR2 fragments and provided a suitable material for further IMAC purification. High yields of the recombinant RyR2 fragments were obtained after elution from Ni-NTA resin of the constructs Trx·RyR2$^{384\text{–}606}$·His$_6$, Trx·RyR2$^{391\text{–}606}$·His$_6$ and Trx·RyR2$^{409\text{–}606}$·His$_6$, Fig. 3D. Surprisingly, in constructs where RyR2 fragments were fused to the NusA protein, Nus·RyR2$^{1\text{–}606}$ and Nus·RyR2$^{230\text{–}606}$, the majority of recombinant protein was found in insoluble form (Fig. 3C).

The overall evaluation of expression and solubility showed that the recombinant N-terminal RyR2 fragments can be expressed in soluble form from the first authentic methionine (RyR2$^{1\text{–}247}$·His$_6$ and RyR2$^{1\text{–}606}$·His$_6$) as well as from the deleted N-terminus where the authentic amino acid sequence is preceded with a methionine (RyR2$^{391\text{–}606}$·His$_6$ and RyR2$^{409\text{–}606}$·His$_6$). N-terminal fusion of RyR2 fragments (Trx·RyR2$^{384\text{–}606}$·His$_6$, Trx·RyR2$^{391\text{–}606}$·His$_6$ and Trx·RyR2$^{409\text{–}606}$·His$_6$) significantly improved expression and solubility of the fragments involving the RIH domain. Ni-NTA eluates of the fragments RyR2$^{1\text{–}606}$·His$_6$, RyR2$^{409\text{–}606}$·His$_6$, Trx·RyR2$^{384\text{–}606}$·His$_6$, Trx·RyR2$^{391\text{–}606}$·His$_6$ and Trx·RyR2$^{409\text{–}606}$·His$_6$ were further analyzed on a size-exclusion chromatography column. Retention times of individual fragments were compared under identical conditions with those of standards. The retention times corresponded to the monomeric forms of RyR2 fragments.

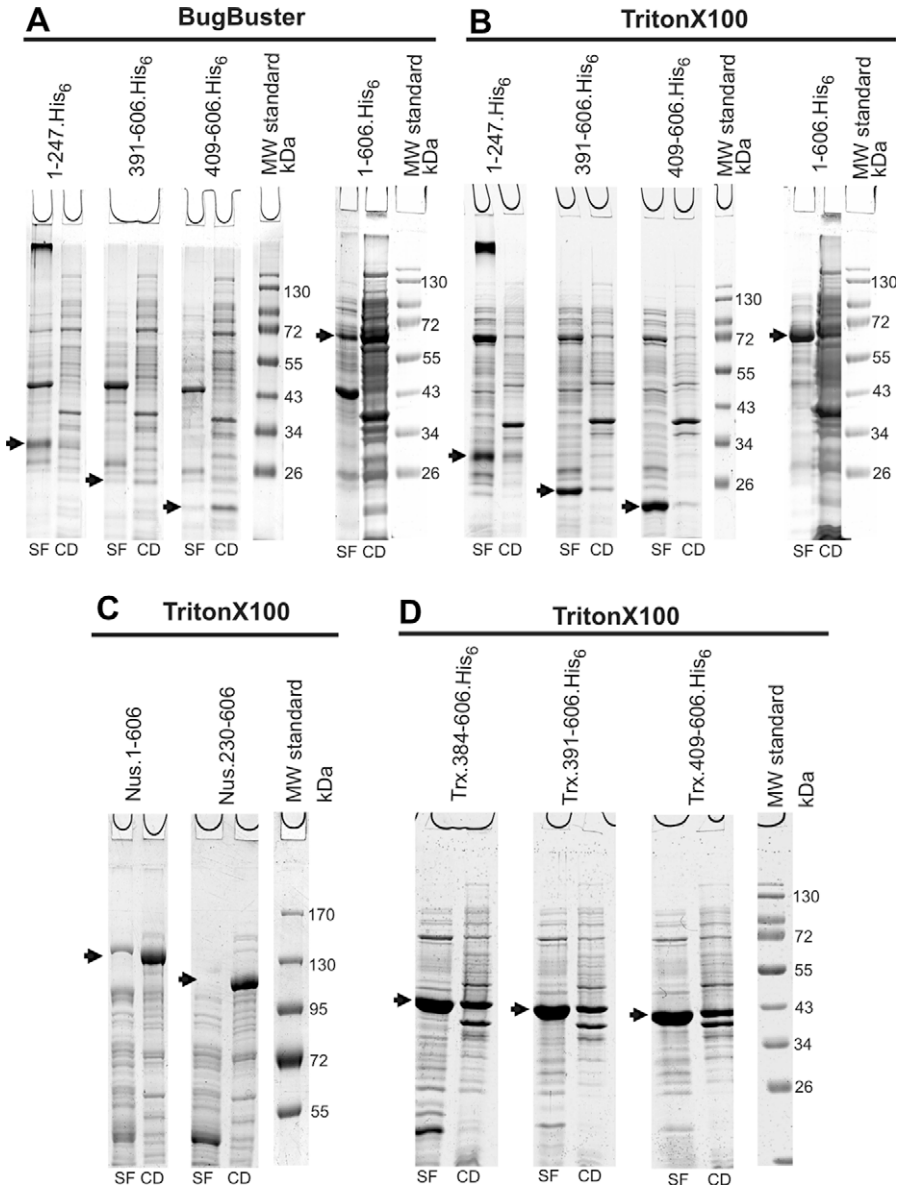

Fig. 3. Solubility of the N-terminal RyR2 fragments. (A) and (B) RyR2$^{1\text{–}247}$·His$_6$, RyR2$^{391\text{–}606}$·His$_6$, RyR2$^{409\text{–}606}$·His$_6$ and RyR2$^{1\text{–}606}$·His$_6$ solubilized with BugBuster and Triton X-100, respectively. (C) Nus·RyR2$^{1\text{–}606}$ and Nus·RyR2$^{230\text{–}606}$ solubilized with Triton X-100 and (D) Trx·RyR2$^{384\text{–}606}$·His$_6$, Trx·RyR2$^{391\text{–}606}$·His$_6$ and Trx·RyR2$^{409\text{–}606}$·His$_6$ solubilized with Triton X-100. SF and CD represent eluates from the Ni-NTA resin and the insoluble cell debris, respectively. Arrowheads indicate the positions of the respective protein bands.

CD spectroscopy

The largest recombinant product RyR2$^{1-606}$·His$_6$ was analyzed by CD spectroscopy. Far-UV spectra showed extrema at 192 and 208 nm as well as a shoulder at 221 nm indicative for a substantial α-helical content (Fig. 4A). Only very small changes were observed within the 4–35 °C temperature range. When rising the temperature further to 40 °C, the protein precipitated irreversibly. Spectra recorded in the presence and absence of 0.5 mM dithiotreitol were identical indicating that any putative disulfide bonds like that between Cys36 and Cys65 as found in the mouse protein [14] have no influence on the secondary structure and stability. Deconvolution of the 4–35 °C spectra showed an α-helix and β-strand content of ~23% and ~29%, respectively. These data are in agreement with sequence based secondary structure predictions, which – dependent of the method used – range from 22% to 44% for α-helices and 16–32% for β-strands. JPRED prediction (Fig. 1B) resulted in a 31% and 24% content of α-helices and β-strands, respectively.

Near-UV CD spectra provide information on the tertiary structure and dynamics. The distinct peaks observed at 285 and 292 nm (Fig. 4B) indicate that some of the 10 tryptophan residues are buried in a nonpolar environment [41] which is in agreement with the mouse RyR2$^{1-217}$ structure showing four tryptophanes within this fragment shielded from solvent exposure [14]. The extrema observed in the 258–270 nm range are probably caused by sterically constraint mobility of some of the 17 phenylalanine residues, although the 266 nm maximum could also arise from a ^1L_a tryptophan transition. The shoulder at 277 nm is indicative for constrained tyrosine side chain mobility [41]. The far- and near-UV CD data suggest that RyR2$^{1-606}$·His$_6$ adopts a defined secondary and tertiary fold, which is in agreement with the sequence analysis data (Fig. 1B) indicating a native-like conformation.

CD-spectroscopy of RyR2$^{1-606}$·His$_6$ fragment was performed also in the presence of ATP which is important activator of RyR channels [42,43]. Therefore, we measured far-UV CD spectra of RyR2$^{1-606}$·His$_6$ after the addition of ATP to final concentrations of 30, 90, 150, 290 and 370 μM at 20 °C. No change of the CD signal could be observed (data not shown). This suggests that ATP does not bind to this fragment of RyR2 with high affinity, or that any conformational changes involved in such interaction are too small to be monitored with this technique.

Limited proteolysis, hybridization and N-terminal sequencing

It is well known that proteases preferentially cleave those parts of a protein that are readily accessible (mainly loops), leaving the well-folded, compact regions of the molecule intact [44]. Therefore, the recombinant fragment RyR2$^{1-606}$·His$_6$ was subjected to proteolytic digestion by trypsin and chymotrypsin to find well-folded regions in the RyR2 fragment and compare them with those predicted by PFAM.

Limited proteolytic digestion by trypsin for 5 and 10 min showed specific cleavage of RyR2$^{1-606}$·His$_6$ into two fragments with a molecular mass of ~40 and 25 kDa. The relative level of the 40 kDa fragment decreased, while that of the 25 kDa fragment increased, with duration of the digestion, Fig. 5A, B, suggesting the greater stability of the smaller fragment. Digestion with chymotrypsin resulted in four discrete fragments, the largest and the smallest having similar molecular weights as those obtained by trypsin digestion, Fig. 5A. This suggests the existence of two well-folded entities in the N-terminus of RyR2. To find out which part of the RyR2$^{1-606}$·His$_6$ was removed, immunodetection with the His·Tag monoclonal antibody was performed on the proteolytic fragments. It was found that all discrete fragments obtained by digestion with trypsin and chymotrypsin contained the C-terminal His·Tag (Fig. 5B), indicating that both proteases specifically digest RyR2$^{1-606}$·His$_6$ from the N-terminus, leaving the C-terminus intact. N-terminal sequencing of the undigested RyR2$^{1-606}$·His$_6$ showed that the first methionine was processed in *E. coli*. The remaining sequence (Table 3) was identical with the prediction deduced from cDNA [2].

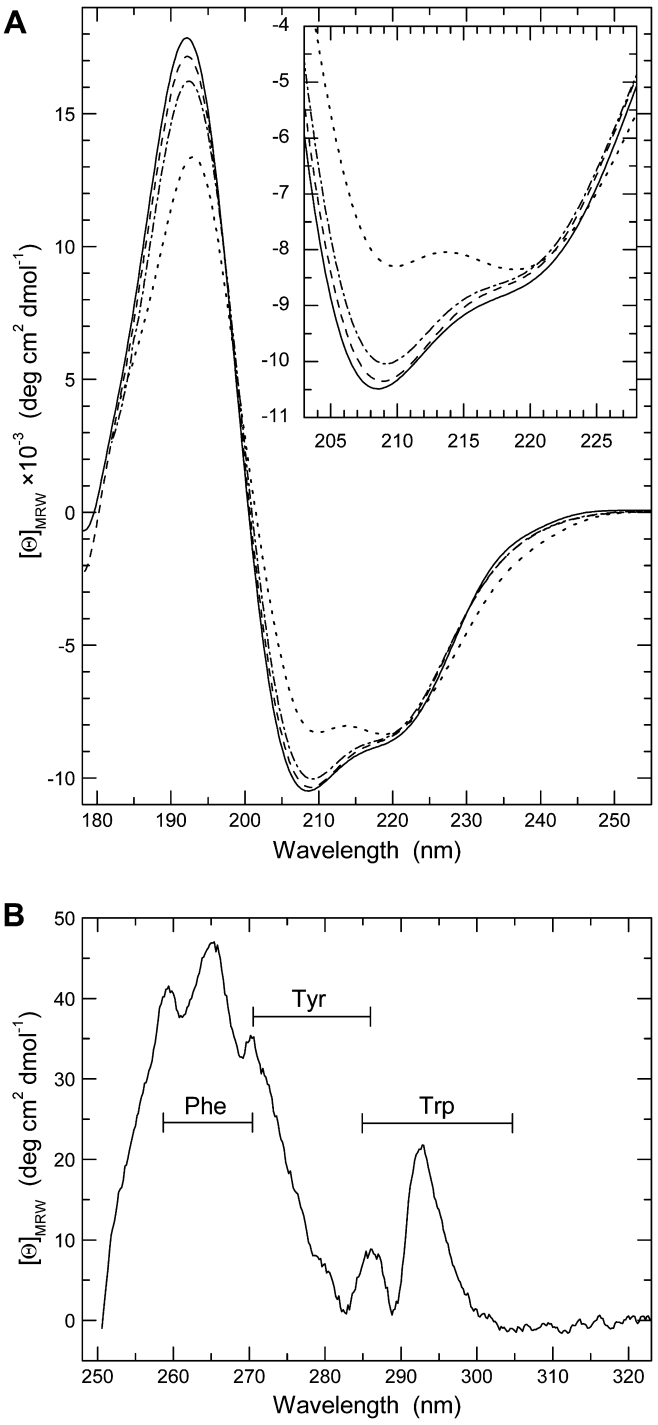

Fig. 4. CD spectra of RyR2$^{1-606}$·His$_6$. Far-UV CD spectra (A) were recorded at increasing temperatures at 4 °C (solid line), 30 °C (dashed line), 35 °C (dash-dotted line) and 40 °C (dotted line, precipitated). The inset shows a magnified view of the $\pi \rightarrow \pi^*$ (208 nm) and $n \rightarrow \pi^*$ (221 nm) transitions characteristic for α-helices. The near-UV spectrum (B) measured at 4 °C shows distinct peaks, which correlate with the ^1L_b transitions of the aromatic residues phenylalanine, tyrosine and tryptophan as indicated by bars suggesting a restricted mobility of some of their side chains.

N-terminal amino acid sequencing of the fragments obtained by limited trypsin proteolysis showed that the larger ~40 kDa fragment starts with Thr259 and the smaller, ~25 kDa fragment, starts

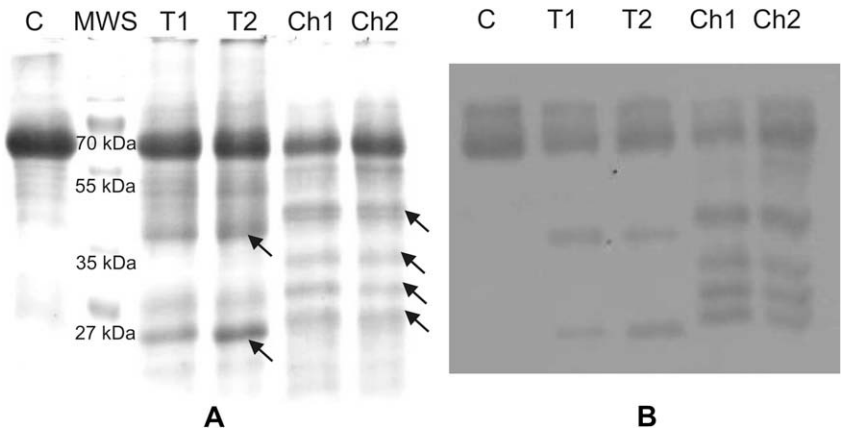

Fig. 5. (A) Proteolytic digestion of fragment RyR2$^{1-606}$·His$_6$ by trypsin (fragments T1 and T2) and chymotrypsin (Ch1 and Ch2) proteases. Samples T1 and Ch1 were digested for 5 min, samples T2 and Ch2 for 10 min, at 25 °C. Sample C is undigested RyR2$^{1-606}$·His$_6$ fragment. (B) Autoradiogram of hybridization of undigested RyR2$^{1-606}$·His$_6$ and digested by trypsin (T1, T2) and chymotrypsin (Ch1, Ch2) with His-Tag monoclonal antibody. Arrows point to the RyR2 fragments obtained by trypsin and chymotrypsin digestion.

Table 3
RyR2$^{1-606}$·His$_6$ and its tryptic digests.

RyR2 fragments (aa residues)	N-terminal aa sequences	M_W – SDS–PAGE [kDa]	Calculated M_W [kDa]
1–606	A, D, G, G, E	~70	68.6
259–606	T, V, H, Y, E	~40	40.3
384–606	M, G, S, I, Q	~25	26.0

Calculated M_W was determined by ProtParam (http://www.expasy.org).

with Met384, Table 3. An arginine precedes both of these residues, which is in agreement with a trypsin cleavage site. Despite the fact that there are several arginines (lysines) in the RyR2$^{1-606}$·His$_6$ sequence, trypsin digestion revealed only two cleavage sites, leading to formation of one main intact region, 384–606, with M_W ~25 kDa. This fragment is identical with the construct no. 6 that was designed according to PFAM, secondary structure prediction and the known structure of IP3R domains, and displayed a high expression level of the recombinant protein Table 2. This fragment contains a part of the MIR domain and the core of the RIH domains. Despite the fact that we did not detect expression of this fragment (construct no. 6), its expression was high when prepared as a fusion protein with thioredoxin, (construct no. 12). Good expression was also detected for the authentic fragment RyR2$^{391-606}$·His$_6$ (construct no. 7), which was shorter than RyR2$^{384-606}$·His$_6$ (construct no. 6) by six residues, as well as for RyR2$^{409-606}$·His$_6$ (construct no. 8) involving the core of RIH domain Fig. 2.

It is interesting to note that the fragment RyR2$^{1-223}$·His$_6$, which corresponds to RyR1$^{1-210}$ [13], showed no expression. However, high expression of the soluble protein was detected for RyR2$^{1-247}$·His$_6$, longer only by 24 residues in comparison to RyR2$^{1-223}$·His$_6$. This suggests that the missing residues are important and probably form a part of a structural segment without which the mRNA or protein is not stable.

Conclusion

We have mapped the N-terminal part of the human cardiac ryanodine receptor (residues 1–759) in order to localize fragments that can be expressed in monomeric, soluble form and behave as independent protein molecules. Bioinformatics prediction using the PFAM database suggested three putative domains. Based on this prediction, 14 expression constructs were prepared, nine of which produced recombinant proteins of the expected size. Six constructs – RyR2$^{1-606}$·His$_6$, RyR2$^{391-606}$·His$_6$, RyR2$^{409-606}$·His$_6$ and Trx·RyR2$^{384-606}$·His$_6$, Trx·RyR2$^{391-606}$·His$_6$, Trx·RyR2$^{409-606}$·His$_6$ – were present in monomeric form after IMAC purification as confirmed by gel filtration chromatography. RyR2$^{1-606}$·His$_6$ was subjected to tryptic digestion giving rise to one stable protein product identified as the predicted fragment RyR2$^{384-606}$·His$_6$. CD spectroscopy indicates that the largest RyR2$^{1-606}$·His$_6$ fragment is folded into native-like form and the content of secondary structure elements is in agreement with that obtained from sequence based predictions.

Acknowledgements

The authors are grateful to Dr. Gabriela Ondrovičová and Dr. Eva Kutejová for their help with proteolysis and western blotting; to Dr. Zdenk Voburka for N-terminal amino acid sequencing and Dr. Jacob Bauer for editing the manuscript. This work was supported by the Slovak Research and Development Agency, Grant APVV-0139-06 and British Heart Foundation Grant PG05077, Grants VEGA 2/0131/10, VEGA 2/0190/10 and EMBO short term fellowship ASTF 27.00-2009 to V.B.-H.

References

[1] Y. Wu, B. Aghdasi, S.J. Dou, J.Z. Zhang, S.Q. Liu, S.L. Hamilton, Functional interactions between cytoplasmic domains of the skeletal muscle Ca^{2+} release channel, J. Biol. Chem. 272 (1997) 25051–25061.
[2] R.E. Tunwell, C. Wickenden, B.M. Bertrand, V.I. Shevchenko, M.B. Walsh, P.D. Allen, F.A. Lai, The human cardiac muscle ryanodine receptor – calcium release channel: identification, primary structure and topological analysis, Biochem. J. 318 (1996) 477–487.
[3] A. Fabiato, Calcium-induced release of calcium from the cardiac sarcoplasmic reticulum, Am. J. Physiol. 245 (1983) C1–14.
[4] J. Fujii, K. Otsu, F. Zorzato, S. de Leon, V.K. Khanna, J.E. Weiler, P.J. O'Brien, D.H. MacLennan, J. Fujii, K. Otsu, Identification of a mutation in porcine ryanodine receptor associated with malignant hyperthermia, Science 253 (1991) 448–451.
[5] Y. Zhang, H.S. Chen, V.K. Khanna, S. De Leon, M.S. Phillips, K. Schappert, B.A. Britt, A.K. Browell, D.H. MacLennan, A mutation in the human ryanodine receptor gene associated with central core disease, Nat. Genet. 5 (1993) 46–50.
[6] S.G. Priori, C. Napolitano, N. Tiso, M. Memmi, G. Vignati, R. Bloise, V. Sorrentino, G.A. Danieli, Mutations in the cardiac ryanodine receptor gene (hRyR2) underlie catecholaminergic polymorphic ventricular tachycardia, Circulation 103 (2001) 196–200.
[7] N. Tiso, D.A. Stephan, A. Nava, A. Bagattin, J.M. Devaney, F. Stanchi, G. Larderet, B. Brahmbhatt, K. Brown, B. Bauce, M. Muriago, C. Basso, G. Thiene, G.A. Danieli, A. Rampazzo, Identification of mutations in the cardiac ryanodine receptor gene in families affected with arrhythmogenic right ventricular cardiomyopathy type 2 (ARVD2), Hum. Mol. Genet. 10 (2001) 189–194.
[8] N. Ikemoto, T. Yamamoto, Regulation of calcium release by interdomain interaction within ryanodine receptors, Front. Biosci. 7 (2002) 671–683.
[9] R. El-Hayek, Y. Saiki, T. Yamamoto, N. Ikemoto, A postulated role of the near amino-terminal domain of the ryanodine receptor in the regulation of the sarcoplasmic reticulum $Ca^{(2+)}$ channel, J. Biol. Chem. 274 (1999) 33341–33347.

[10] T. Yamamoto, N. Ikemoto, Peptide probe study of the critical regulatory domain of the cardiac ryanodine receptor, Biochem. Biophys. Res. Commun. 291 (2002) 1102–1108.
[11] A. Shtifman, C.W. Ward, T. Yamamoto, J. Wang, B. Olbinski, H.H. Valdivia, N. Ikemoto, M.F. Schneider, Interdomain interactions within ryanodine receptors regulate Ca^{2+} spark frequency in skeletal muscle, J. Gen. Physiol. 119 (2002) 15–32.
[12] M. Yano, T. Yamamoto, Y. Ikeda, M. Matsuzaki, Mechanisms of disease: ryanodine receptor defects in heart failure and fatal arrhythmia, Nat. Clin. Pract. Cardiovasc. Med. 3 (2006) 43–52.
[13] F.J. Amador, S. Liu, N. Ishiyama, M.J. Plevin, A. Wilson, D.H. MacLennan, M. Ikura, Crystal structure of type I ryanodine receptor amino-terminal beta-trefoil domain reveals a disease-associated mutation "hot spot" loop, Proc. Natl. Acad. Sci. USA 106 (2009) 11040–11044.
[14] P.A. Lobo, F. Van Petegem, Crystal structures of the N-terminal domains of cardiac and skeletal muscle ryanodine receptors: insights into disease mutations, Structure 17 (2009) 1505–1514.
[15] S. Jana, J.K. Deb, Strategies for efficient production of heterologous proteins in *Escherichia coli*, Appl. Microbiol. Biotechnol. 67 (2005) 289–298.
[16] P. Braun, J. LaBaer, High throughput protein production for functional proteomics, Trends Biotechnol. 21 (2003) 383–388.
[17] W. Peti, R. Page, Strategies to maximize heterologous protein expression in *Escherichia coli* with minimal cost, Protein Expression Purif. 51 (2007) 1–10.
[18] N.S. Berrow, K. Bussow, B. Coutard, J. Diprose, M. Ekberg, G.E. Folkers, N. Levy, V. Lieu, R.J. Owens, Y. Peleg, C. Pinaglia, S. Quevillon-Cheruel, L. Salim, C. Scheich, R. Vincentelli, D. Busso, Recombinant protein expression and solubility screening in *Escherichia coli*: a comparative study, Acta Crystallogr. D62 (2006) 1218–1226.
[19] F. Baneyx, Recombinant protein expression in *Escherichia coli*, Curr. Opin. Biotechnol. 10 (1999) 411–421.
[20] T. Cornvik, S.L. Dahlroth, A. Magnusdottir, S. Flodin, B. Engvall, V. Lieu, M. Ekberg, P. Nordlund, An efficient and generic strategy for producing soluble human proteins and domains in *E Coli* by screening construct libraries, Proteins 65 (2006) 266–273.
[21] A. Vera, N. Gonzalez-Montalban, A. Aris, A. Villaverde, The conformational quality of insoluble recombinant proteins is enhanced at low growth temperatures, Biotechnol. Bioeng. 96 (2007) 1101–1106.
[22] G.D. Davis, C. Elisee, D.M. Newham, R.G. Harrison, New fusion protein systems designed to give soluble expression in *Escherichia coli*, Biotechnol. Bioeng. 65 (1999) 382–388.
[23] M.R. Sharma, P. Penczek, R. Grassucci, H.B. Xin, S. Fleischer, T. Wagenknecht, Cryoelectron microscopy and image analysis of the cardiac ryanodine receptor, J. Biol. Chem. 273 (1998) 18429–18434.
[24] C.H. George, H. Jundi, N.L. Thomas, D.L. Fry, F.A. Lai, Ryanodine receptors and ventricular arrhythmias: emerging trends in mutations, mechanisms and therapies, J. Mol. Cell. Cardiol. 42 (2007) 34–50.
[25] R. Stewart, S. Zissimopoulos, F.A. Lai, Oligomerization of the cardiac ryanodine receptor C-terminal tail, Biochem. J. 376 (2003) 795–799.
[26] G.C. Chan, J.T. Yang, Two-point calibration of circular dichrometer with d-10-camphorsulfonic acid, Anal. Lett. 10 (1977) 1195–1208.
[27] C.N. Pace, F. Vajdos, L. Fee, G. Grimsley, T. Gray, How to measure and predict the molar absorption coefficient of a protein, Protein Sci. 11 (1995) 2411–2423.
[28] W.C. Johnson Jr., Analysing protein circular dichroism spectra for accurate secondary structures, Proteins 35 (1999) 307–312.
[29] L. Whitmore, B.A. Wallace, DICHROWEB, an online server for protein secondary structure analyses from circular dichroism spectroscopic data, Nucl. Acids Res. 32 (2004) 668–673.
[30] J.G. Lees, A.J. Miles, F. Wien, B.A. Wallace, A reference database for circular dichroism spectroscopy covering fold and secondary structure space, Bioinformatics 22 (2006) 1955–1962.
[31] R.D. Finn, J. Tate, J. Mistry, P.C. Coggill, S.J. Sammut, H.R. Hotz, G. Ceric, K. Forslund, S.R. Eddy, E.L. Sonnhammer, A. Bateman, The Pfam protein families database, Nucl. Acids Res. 36 (2008) D 281–288.
[32] C.P. Ponting, Novel repeats in ryanodine and IP3 receptors and protein *O*-mannosyltransferases, Trends Biochem. Sci. 25 (2000) 48–50.
[33] I. Bosanac, H. Yamazaki, T. Matsu-Ura, T. Michikawa, K. Mikoshiba, M. Ikura, Crystal structure of the ligand binding suppressor domain of type 1 inositol 1, 4, 5-trisphosphate receptor, Mol. Cell. 17 (2005) 193–203.
[34] I. Bosanac, J.R. Alattia, T.K. Mal, J. Chan, S. Talarico, F.K. Tong, K.I. Tong, F. Yoshikawa, T. Furuichi, M. Iwai, T. Michikawa, K. Mikoshiba, M. Ikura, Structure of the inositol 1, 4, 5-trisphosphate receptor binding core in complex with its ligand, Nature 420 (2002) 696–700.
[35] S.O. Marx, S. Reiken, Y. Hisamatsu, M. Gaburjakova, J. Gaburjakova, Y.M. Yang, N. Rosemblit, A.R. Marks, Phosphorylation-dependent regulation of ryanodine receptors: a novel role for leucine/isoleucine zippers, J. Cell. Biol. 153 (2001) 699–708.
[36] S. Strahl-Bolsinger, A. Scheinost, Transmembrane topology of pmt1p, a member of an evolutionarily conserved family of protein *O*-mannosyltransferases, J. Biol. Chem. 274 (1999) 9068–9075.
[37] T. Hamada, K. Tashiro, H. Tada, J. Inazawa, M. Shirozu, K. Shibahara, T. Nakamura, N. Martina, T. Nakano, T. Honjo, Isolation and characterization of a novel secretory protein, stromal cell-derived factor-2 (SDF-2) using the signal sequence trap method, Gene 176 (1996) 211–214.
[38] A.G. Murzin, A.M. Lesk, C. Chothia, Beta-trefoil fold. Patterns of structure and sequence in the Kunitz inhibitors interleukins-1 beta and 1 alpha and fibroblast growth factors, J. Mol. Biol. 223 (1992) 531–543.
[39] C. Cole, J.D. Barber, G.J. Barton, The Jpred 3 secondary structure prediction server, Nucl. Acids Res. 36 (2008) 197–201.
[40] J.G. Marblestone, S.C. Edavettal, Y. Lim, P. Lim, X. Zuo, T.R. Butt, Comparison of SUMO fusion technology with traditional gene fusion systems: enhanced expression and solubility with SUMO, Protein Sci. 15 (2006) 182–189.
[41] E.H. Strickland, Aromatic contributions to circular dichroism spectra of proteins, C.R.C. Crit. Rev. Biochem. 2 (1974) 113–175.
[42] A.F. Dulhunty, P. Pouliquin, M. Coggan, P.W. Gage, P.G. Board, A recently identified member of the glutathione transferase structural family modifies cardiac RyR2 substrate activity, coupled gating and activation by Ca^{2+} and ATP, Biochem. J. 390 (2005) 333–343.
[43] R. Bull, J.P. Finkelstein, A. Humeres, M.I. Behrens, C. Hidalgo, Effects of ATP, Mg^{2+}, and redox agents on the Ca^{2+} dependence of RyR channels from rat brain cortex, Am. J. Physiol. Cell Physiol. 293 (2007) C162–C171.
[44] I.F. Chang, Mass spectrometry-based proteomic analysis of the epitope-tag affinity purified protein complexes in eukaryotes, Proteomics 6 (2006) 6158–6166.